

## *In Situ* Discovery of an Electrostatic Potential, Trapping Electrons and Mediating Fast Reconnection in the Earth's Magnetotail

J. Egedal,<sup>1</sup> M. Øieroset,<sup>2</sup> W. Fox,<sup>1</sup> and R. P. Lin<sup>2,3</sup>

<sup>1</sup>Massachusetts Institute of Technology, Plasma Science Fusion Center, Cambridge, Massachusetts 02139, USA

<sup>2</sup>Space Sciences Laboratory, University of California, Berkeley, California 94720, USA

<sup>3</sup>Physics Department, University of California, Berkeley, California 94720, USA

(Received 11 February 2004; revised manuscript received 10 August 2004; published 19 January 2005)

Anisotropic electron phase space distributions,  $f$ , measured by the Wind spacecraft in a rare crossing of a diffusion region in Earth's far magnetotail (60 Earth radii), are analyzed. We use the measured  $f$  to probe the electrostatic and magnetic geometry of the diffusion region. For the first time, the presence of a strong electrostatic potential (1 kV) within the ion diffusion region is revealed. This potential has far reaching implications for the reconnection process; it accounts for the observed acceleration of the unmagnetized ions out of the reconnection region and it causes all thermal electrons be trapped electrostatically. The trapped electron motion implies that the thermal part of the electron distributions are symmetric around  $v_{\parallel} = 0$ :  $f(v_{\parallel}, v_{\perp}) \approx f(-v_{\parallel}, v_{\perp})$ . It follows that the field aligned currents in the diffusion region are limited and fast magnetic reconnection is mediated.

DOI: 10.1103/PhysRevLett.94.025006

PACS numbers: 94.30.-d, 52.20.-j, 52.35.Vd

Magnetic reconnection, the process in a plasma during which magnetic field lines rearrange and change topology [1,2], plays a fundamental role in a variety of plasma phenomena. It controls the evolution of solar flares [3], it allows the solar Wind to enter Earth's magnetosphere [4], and it is an integral part of magnetic substorms and the aurora phenomena [5,6]. Mounting evidence suggests that the fast rate at which reconnection proceeds is strongly influenced by the ion-scale Hall effect [7]. However, for fast reconnection to be maintained, a hitherto unknown electron scale process must limit the electron current in the reconnection region, allowing electrons to diffuse through the magnetic field at the same or at even a higher rate than the ions [8].

Recently, the first *in situ* measurements of the electron distribution function have been reported for a reconnection event encountered by the Wind spacecraft in Earth's magnetotail [9,10]. This event, observed in the deep magnetotail (60 Earth radii), is characterized by a kinetic regime in which the electron temperature is high,  $T_e \sim 400$  eV, and the magnetic field is weak,  $B = 6\text{--}12$  nT, implying an electron thermal speed,  $v_{th}$ , much larger than the Alfvén speed,  $v_A$  (for the observed density  $n = 0.1$  cm<sup>-3</sup>), and thus larger than the outflow speed,  $v_{out}$ , of plasma from the reconnection region.

Because of the computational requirements posed by this kinetic regime ( $v_{th} \sim 40v_{out}$ ), so far it has not been accessible to self-consistent particle simulations. Meanwhile, in Ref. [11] the regime was investigated through the use of Liouville's theorem applied to the electron trajectories in prescribed fields. This technique of following particle trajectories for understanding particle distribution functions measured in space was pioneered by Speiser [12] and has since been applied in numerous investigations [13–16]. More recently, prompted by experimental observation in the Versatile Toroidal Facility (VTF) magnetic

reconnection experiment, the kinetic regime was also studied in Ref. [17]. Applying an approach similar to those in Refs. [11,17], the Wind electron distributions are used to “probe” the electrostatic and the magnetic geometry of the reconnection region; the presence of a strong electrostatic potential ( $\sim 1$  kV) is revealed. This potential causes all thermal electrons to follow trapped trajectories inside the reconnection region, significantly limiting the number of “free” current carriers. As has been proven experimentally at the VTF [18,19], the trapped orbit dynamics effectively mediates fast reconnection.

Figure 1 illustrates the ion flow, magnetic field components, and plasma density measured by Wind during its fortunate encounter with the reconnection region. The gradual ion flow reversal and the measured magnetic field components, including Hall-current-generated out-of-plane ( $B_y$ ) magnetic fields, indicate that Wind passed through the ion diffusion region of a quasisteady collisionless reconnection region [9,10]. Based on these measurements and assuming a magnetic X-line structure as characteristic for reconnection, the approximate path of Wind through the diffusion region can be reconstructed as shown in the schematic of Fig. 2(a).

Examples of electron distributions measured as Wind passed through the ion diffusion region are displayed in Figs. 3(a)–3(c). The measurements provide the phase-space density,  $f$ , of the electrons as a function of pitch angle,  $\theta = \angle(\mathbf{v}, \mathbf{B})$ , and kinetic energy,  $\mathcal{E}_k$ . The anisotropy is most pronounced in the distribution shown in Fig. 3(a), which was obtained near the center of the diffusion region. The anisotropy gradually decreases as Wind exits the X-line region [Figs. 3(b) and 3(c)].

Because the Coulomb collision frequency of the electrons,  $\nu \sim 10^{-9}$  s<sup>-1</sup>, is very small compared to any other frequency in the magnetotail,  $f$  is governed by the collisionless Vlasov equation  $df/dt = 0$ . Here  $d/dt$  represents

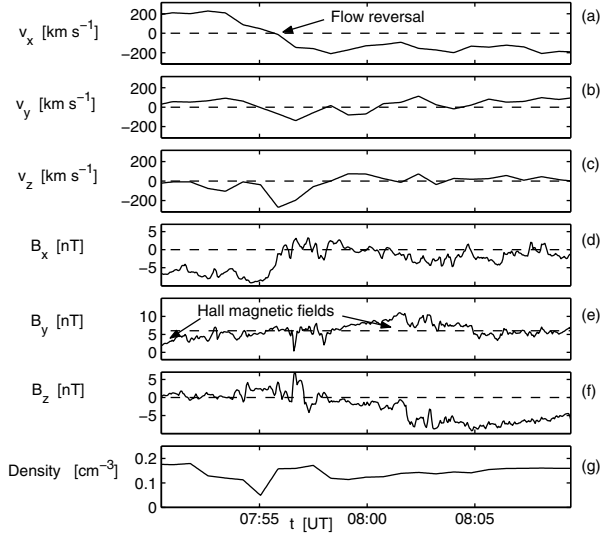


FIG. 1. Wind measurements of the ion flow, the magnetic field components, and density during the encounter with an active reconnection region. Further away from the  $X$  line  $v_y$  and  $v_z$  remain small, while the ion outflow speed,  $|v_x|$ , approaches the Alfvén speed of 400 km/s.

the total time derivative along particle orbits. The Vlasov equation states that the distribution is constant along particle orbits through phase-space  $(\mathbf{x}, \mathbf{v})$ . Hence, we can equate  $f$  for a point  $(\mathbf{x}_0, \mathbf{v}_0)$  in the reconnection region to

the isotropic distribution,  $f_\infty$ , in the ambient plasma sheet outside the ion diffusion region, by following particle orbits back in time until they reach points  $(\mathbf{x}_1, \mathbf{v}_1)$  in the sheet. It then follows that

$$f(\mathbf{x}_0, \mathbf{v}_0) = f_\infty(v_1), \quad v_1 = |\mathbf{v}_1|. \quad (1)$$

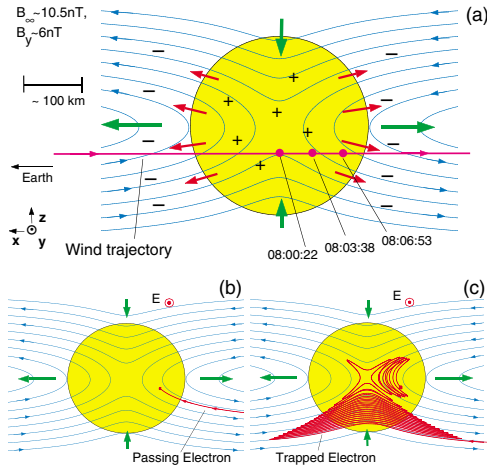


FIG. 2 (color). (a) Illustration of the magnetic geometry and the trajectory of Wind. The green arrows indicate the flow of magnetic flux towards and away from the  $X$  line. At locations away from the  $X$  line the in-plane magnetic field approaches values of about 10 nT. Besides the in-plane magnetic fields, an out-of-plane guide magnetic field,  $B_y = 6$  nT, was also observed. The red arrows illustrate the electrostatic electric field trapping the thermal electrons within the ion diffusion region (the yellow area). (b) An example of a passing electron guiding center trajectory reaching the location of the Wind spacecraft. (c) An example of a trapped electron trajectory. The electron bounces back and forth along a field line, while slowly drifting with the magnetic field towards the  $X$  line.

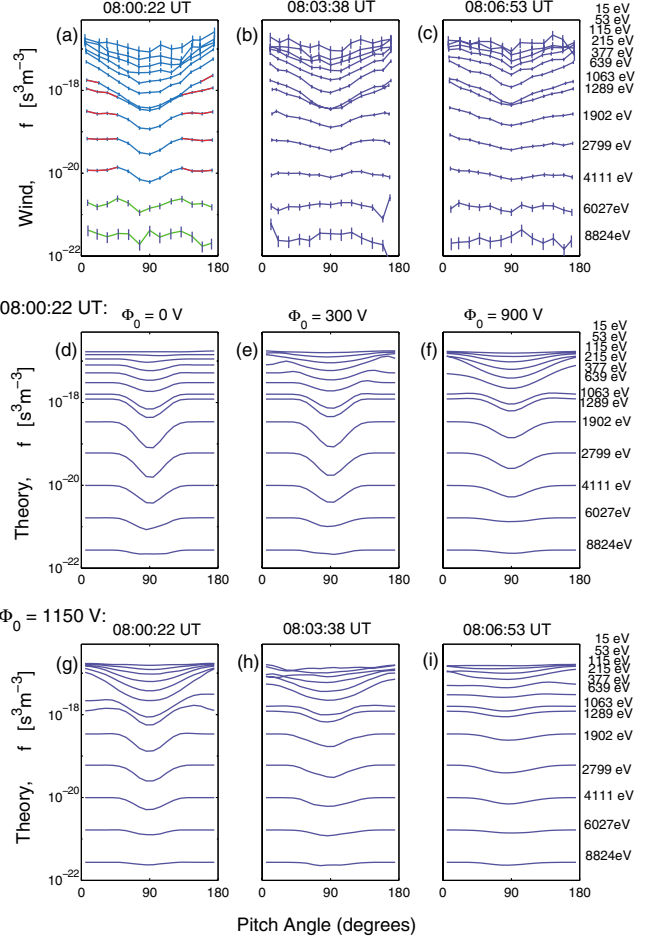


FIG. 3 (color). (a)–(c) Electron pitch angle distributions measured by the 3D plasma and energetic particle instrument [25] on the Wind spacecraft at locations indicated in Fig. 2. Each line represents the phase-space density for a given energy; the respective energies are given on the right of the figure. In (a) the blue parts correspond to trapped electrons, and the red parts correspond to passing electrons. At sufficiently high energies the electron orbits become unmagnetized, leading to pitch angle scattering; this effect reduces the level of anisotropy observed above 6 keV [the green parts in (a)]. (d)–(i) Theoretical distributions calculated for locations [inferred from the measured values of  $(B_x, B_z)$ ] corresponding to the data in (a)–(c). The distributions in (d)–(g) correspond to the center of the diffusion region ( $t = 08:00:22$ UT) calculated with increasing values of the trapping potential ( $\Phi_0 \in \{0, 300, 900, 1150\}$  V). The best match to the data in Fig. 3(a) is obtained with  $\Phi_0 = 1150$  V. The distributions in (h) and (i), also obtained with  $\Phi_0 = 1150$  V, correspond to the Wind observations in the outflow region [see (b) and (c)].

The measured distributions are therefore closely related to changes in kinetic energy that the particles undergo along their trajectories into the  $X$ -line region.

The electrons can reach the  $X$ -line region via two distinct types of trajectories: passing and trapped. An example of a passing trajectory is shown in Fig. 2(b). The passing electron reaches the location of the measurement along a field line. Electrons of this type (if not intercepted by the spacecraft) continue to follow the magnetic field line out of the region, without experiencing any significant changes in energy.

An example of a trapped electron is given in Fig. 2(c). In their rapid bounce motion back and forth along field lines, the total energy is conserved. Consequently, the variations in the kinetic energy during the bounce motion are linked to the variations in the electrostatic potential along the field lines. Thus, the trapping of electrons is a consequence of the electric field structure in the reconnection region as well as the local minimum in the magnetic field strength.

The evolution of the kinetic energy in the slower motion where the trapped electrons drift with the magnetic field towards the  $X$  line is governed by adiabatic invariance. For thermal electrons the magnetic moment,  $\mu = mv_{\perp}^2/(2B)$ , and the second adiabatic invariant of the bounce motion,  $J = \oint v_{\parallel} dl$ , are conserved [17]. The conservation of  $\mu$  and the decrease in  $B$  as the  $X$  line is approached causes a decrease in  $v_{\perp}^2$  [11,13]. Meanwhile, an increase is observed in  $v_{\parallel}$ , which is due to the conservation of  $J$  and the decreasing orbit bounce length ( $\oint dl$ ) in the inflow region. The combination gives particles with  $v_{\parallel} \geq v_{\perp}$  ( $v_{\parallel} \leq v_{\perp}$ ) a net gain (loss) in  $\mathcal{E}_k$  in the inflow region.  $B_y$  is large enough that  $\mu$  is conserved for thermal electrons at all locations, and no pitch angle diffusion is observed at the  $X$  line. In the outflow region the changes in  $\mathcal{E}_k$  are reversed. The trapped orbit motion also implies that  $f$  is nearly symmetric in pitch angle around  $90^\circ$ :  $f(v, \Theta) = f(v, 180^\circ - \Theta)$  [16].

For sufficiently high energies ( $\mathcal{E}_k > 1$  keV) only the magnetic forces are important in determining if an electron is trapped or passing. The flat parts of the distribution in Fig. 3(a), indicated by the red lines, correspond to passing orbits, whose energies do not change on the path from the ambient plasma. The blue parts are associated with trapped electrons; the dip in phase-space density as a function of  $\theta$  is caused by the cooling of these electrons in the inflow region. This interval of trapped electrons is determined by the magnetic field strength,  $B_y = 6$  nT, along the  $X$  line and the asymptotic value,  $B_{\infty} = 10.5$  nT, away from the  $X$  line. From the finite ratio  $B_y/B_{\infty}$ , standard magnetic mirror trapping arguments predict a phase-space boundary between passing and trapped particles (a loss-cone boundary) at the pitch angles,  $\theta_b \sim 49^\circ$  and  $\theta_b \sim 131^\circ$ . These boundaries agree with the interval covered by the dips in  $f$ .

For the bulk portion of the distribution ( $\mathcal{E}_k \leq 639$  eV) the dips in phase-space density extend from  $\theta = 0^\circ$  to  $\theta =$

$180^\circ$ . This is evidence that the bulk electrons, at *all* pitch angles, enter the  $X$ -line region along trapped trajectories. The broadening of the interval for trapping implies the presence of an electrostatic potential,  $\Phi_{\text{trap}}$ , that traps all thermal electrons.

In the remaining part of this Letter, we describe our theoretical modeling of the measured distributions. The magnetic geometry close to the  $X$  line is approximated by  $\mathbf{B} = b_0[(z/\alpha)\hat{\mathbf{x}} + \alpha x\hat{\mathbf{z}} + l_0\hat{\mathbf{y}}]$ . Consistent with the Wind magnetic field measurements (see Fig. 1) we apply  $B_y = b_0 l_0 = 6$  nT, and  $l_0 = 65$  km. The case with  $\alpha = 1$  corresponds to a currentless cusp for which the angle of the separatrix is  $90^\circ$  (the equation of the separatrix is  $|z| = |\alpha^2 x|$ ). For other values of  $\alpha$  the separatrices meet at some other angle. Several values of  $\alpha$  have been applied in our modeling scheme; the results prove to be independent of this parameter. For simplicity, here we consider a configuration with  $\alpha = 1$ . The electric fields are approximated by  $\mathbf{E} = -\nabla\Phi(x, z) + E_y\hat{\mathbf{y}}$ . Here  $\Phi = \Phi_{\text{rec}} + \Phi_{\text{trap}}$ , where  $\Phi_{\text{trap}} = \Phi_0 \exp[-(x^2 + z^2)/l_0^2]$  is the potential incorporated to trap the thermal electrons. The reconnection rate is estimated by assuming that  $v_{\text{inflow}} = 0.1v_A$ , from which we find  $E_y \sim 0.1 \times 400$  km/s  $\times 6$  nT = 0.24 mV/m (note that our results are insensitive to  $E_y$ ). The role of  $\Phi_{\text{rec}} = \frac{1}{4}l_0 E_y \log[(x^2 + \delta^2)/(z^2 + \delta^2)]$  is to ensure that  $\mathbf{E} \cdot \mathbf{B} \sim 0$  (required from  $\mathbf{E} + \mathbf{v} \times \mathbf{B} = 0$ ) outside the electron diffusion region [17]. We apply a recent experimental result that the size  $\delta$  of the diffusion region scales with the drift orbit width of the trapped electrons,  $\delta = \rho_c = \sqrt{mv_{\text{th}}/(qb_0)} = 10$  km [18] (the length scale  $\rho_c$  has also been found applicable to configurations without a guide magnetic field [20]). The potential  $\Phi_{\text{rec}} \sim l_0 E_y \sim 15$  V is small compared to the electron temperature (400 eV), and the theoretical distributions are therefore nearly independent of  $\Phi_{\text{rec}}$  and  $\delta$ .

We assume that the electrons have reached a point  $\mathbf{x}_1$  outside the  $X$ -line region when  $B(\mathbf{x}_1) = B_{\infty}$ . Hence, orbits are followed back in time from their initial locations  $(\mathbf{x}_0, \mathbf{v}_0)$  to the first location,  $(\mathbf{x}_1, \mathbf{v}_1)$ , for which  $b_0\sqrt{x_1^2 + z_1^2 + l_0^2} = B_{\infty}$ , where  $\mathbf{x}_1 = (x_1, y_1, z_1)$ . The ambient plasma sheet is approximated by an isotropic distribution  $f_{\infty}(|\mathbf{v}_1|)$ , with a temperature of  $T_e \sim 400$  eV for the bulk electrons and a power law dependence,  $f \propto E^{-4.5}$ , for the high energy tail,  $\mathcal{E}_k > 2$  keV, consistent with Wind measurements away from the diffusion region. Additional simulations (not included here) show that the fluctuation level in the magnetic field observed in Fig. 1 does not influence the results of our analysis.

Figures 3(d)–3(g) represent theoretical distributions corresponding to the Wind measurements at time 08:00:22 where Wind was near the center of the diffusion region. These theoretical distributions are obtained with increasing values of the trapping potential ( $\Phi_0 \in \{0, 300, 900, 1150\}$  V). As seen, the measured distributions

are best matched for  $\Phi_0 = 1150$  V. The value  $\Phi_0 = 1150$  V was also applied in calculating the distributions in Figs. 3(h) and 3(i) corresponding to the location of Wind for times 08:03:38 and 08:06:53. The agreement between observations [Figs. 3(a)–3(c)] and model [Figs. 3(g)–3(i)] covers several points which support the present interpretation:

(i) For  $\mathcal{E}_k > 1$  keV, the width and the depth of the dips in the theoretical phase-space density are highly sensitive to the ratio of  $B_y/B_\infty$ ; agreement between the measured  $f$  and the theoretical  $f$  is obtained only when the measured values of  $B_y$  and  $B_\infty$  are used in the simulation.

(ii) The theoretical anisotropy agrees with the measurements not only near the center of the diffusion region, but also at locations in the outflow region; compare Figs. 3(b) and 3(c) with Figs. 3(h) and 3(i).

(iii) For  $\mathcal{E}_k < 1$  keV, agreement with the measured distributions are obtained by including an electrostatic potential,  $\Phi_{\text{trap}}$ , whose strength is uniquely determined by the anisotropy in the electrons. Furthermore, the energy gained by the unmagnetized ions in their acceleration in the outflow region agree with  $\Phi_{\text{trap}}$ . For the applied electrostatic geometry, the potential drop from the center to the edge of the simulation region is about 1000 V. The reported outflow speed of the ions,  $v_{\text{ion,out}} \sim 400$  km/s [10], corresponds to acceleration in a potential drop of  $\sim 835$  V. This suggests that  $\Phi_{\text{trap}}$  is responsible (and adequate) for accelerating the unmagnetized ions out of the X-line region. Such electrostatic structures have also been observed in self-consistent particle simulations [21] (but were not associated with trapping because  $v_{\text{th}} \sim v_{\text{out}}$ ).

(iv) For electrons with energies above 6 keV, the Larmor radii of the electrons are larger than the characteristic length scale of the magnetic field curvature,  $l_0$ . Thus, these electrons see significant changes in  $\mathbf{B}$  over a single Larmor period which causes pitch angle diffusion [22]. Such non-adiabatic effects are evident in both the measured and the theoretical distributions: the levels of anisotropy decrease rapidly above 4 keV.

(v) Inside the ion diffusion region the trapped electrons bounce back and forth along field lines while drifting with the magnetic field. They remain “frozen in” to the magnetic field to within the length scale  $\rho_c$  from the X line. Thus, the electron dynamics are consistent with the Hall magnetic field evident in Fig. 1 and discussed in Ref. [9].

Simulations with  $v_{\text{th}} \sim v_{\text{out}}$  [7,21,23,24] do not capture the electron dynamics evident in the Wind measurements: the electrons do not have time to bounce back and forth along the field lines, so theoretical distributions, in general, will not display the observed symmetry (typically in these simulations  $j_{\parallel} \sim qnv_{\text{th}}$ ). However, the regime  $v_{\text{th}} \sim v_{\text{out}}$  is likely to be relevant for reconnection sites closer to Earth (characterized by higher values of  $B$  and lower  $n_{\text{inflow}}$  producing a higher  $v_A$ ).

In summary, we have applied the electron phase-space distributions  $f$ , measured by Wind within a reconnection region in Earth’s magnetotail, to infer properties of the electrostatic geometry inside the ion diffusion region. For the first time, the presence of a strong electrostatic potential, trapping all thermal electrons, is revealed. The symmetric properties of  $f$  associated with trapping can be expressed as  $f(v_{\parallel}, v_{\perp}) \sim f(-v_{\parallel}, v_{\perp})$ . It follows that  $j_{\parallel} = q \int v_{\parallel} f(v_{\parallel}, v_{\perp}) dv^3 \ll qnv_{\text{th}}$ , which allows the plasma to support an electric field along the X line, mediating fast reconnection [17,19]. Additional investigations in the regime  $v_{\text{th}} \gg v_{\text{out}}$ , numerical as well as experimental, are needed to determine how the trapped orbit dynamics translate into dissipation free  $\nabla \cdot \mathbf{P}$  and  $\mathbf{v} \cdot \nabla \mathbf{j}$  terms in the generalized Ohm’s law.

This work is partly funded by NSF/DOE Grant No. DE-FG02-03ER54712 at MIT and NASA Grants No. NAG5-12941 and No. NAG5-10428 at U.C. Berkeley.

- 
- [1] V.M. Vasyliunas, *Rev. Geophys. Space Phys.* **13**, 303 (1975).
  - [2] E. Priest and T. Forbes, *Magnetic Reconnection* (Cambridge University Press, Cambridge, 2000).
  - [3] R.G. Giovanelli, *Nature (London)* **158**, 81 (1946).
  - [4] B.U.O. Sonnerup *et al.*, *Fluid Aspects of Reconnection at the Magnetopause: In Situ Observations, Physics of the Magnetopause*, Geophysical Monograph Series Vol. 90 (AGU, Washington, DC, 1995), p. 167.
  - [5] B. Coppi *et al.*, *Phys. Rev. Lett.* **16**, 1207 (1966).
  - [6] T. Nagai *et al.*, *J. Geophys. Res.* **106**, 25 929 (2001).
  - [7] J. Birn *et al.*, *J. Geophys. Res.* **106**, 3715 (2001).
  - [8] J.D. Scudder *et al.*, *J. Geophys. Res.* **107**, 1294 (2002).
  - [9] M. Øieroset *et al.*, *Nature (London)* **412**, 414 (2001).
  - [10] M. Øieroset *et al.*, *Phys. Rev. Lett.* **89**, 195001 (2002).
  - [11] G.R. Burkhart *et al.*, *J. Geophys. Res.* **95**, 18 833 (1990).
  - [12] T.W. Speiser, *J. Geophys. Res.* **70**, 4219 (1965).
  - [13] S.V. Bulanov and P.V. Sasorov, *Sov. Astron. J.* **19**, 464 (1976).
  - [14] D.J. Williams and T.W. Speiser, *J. Geophys. Res.* **86**, 5507 (1981).
  - [15] S.V. Bulanov and F. Cap, *Sov. Astron. J.* **32**, 436 (1988).
  - [16] D.B. Curran and C.K. Goertz, *J. Geophys. Res.* **94**, 272 (1989).
  - [17] J. Egedal, *Phys. Plasmas* **9**, 1095 (2002).
  - [18] J. Egedal *et al.*, *Phys. Rev. Lett.* **90**, 135003 (2003).
  - [19] J. Egedal *et al.*, *Phys. Plasmas* **11**, 2844 (2004).
  - [20] G.R. Laval *et al.*, *Plasma Phys. Controlled Nucl. Fusion Res.* **2**, 259 (1966).
  - [21] P.L. Pritchett, *J. Geophys. Res.* **106**, 3783 (2001).
  - [22] J. Egedal and A. Fasoli, *Phys. Plasmas* **8**, 4042 (2001).
  - [23] Z.W. Ma and A. Bhattacharjee, *J. Geophys. Res.* **106**, 3773 (2001).
  - [24] M.A. Shay *et al.*, *Geophys. Res.* **106**, 3759 (2001).
  - [25] R.P. Lin *et al.*, *Space Sci. Rev.* **71**, 125 (1995).